The Treatment of Singularities at 90° and 270° Microstrip Corners in FDTD by the Modification of Assigned Material Parameters

C. J. Railton, D. L. Paul, I. J. Craddock, and G. S. Hilton

***Abstract*—It has been recently shown that the efficiency of the finite-difference time-domain (FDTD) method for structures containing thin wires and metal edges is much increased by using modified assigned material parameters (MAMPs). These parameters may be calculated empirically and in many cases analytically. In this contribution, the technique is extended to include the case of 90° and 270° corners in microstrip which may exist at an arbitrary position within the plane of the mesh. A semi-analytical method is presented and applied to the analysis of a complex patch antenna. Results are presented which show that the use of MAMPs allows a much larger cell size to be used than would be needed to achieve the same accuracy using standard FDTD.**

***Index Terms*—Finite-difference time-domain (FDTD) methods, planar objects, planar waveguides.**

I. Introduction

It was shown in [1], [2] and [3] that the effects of field singularities in the region of wires and strips can be accounted for within the FDTD method, by altering the permittivities and permeabilities assigned to the neighboring E and H field nodes. In many situations, the required values for these modified assigned material parameters (MAMPs) can be derived analytically. It was demonstrated in [2] that the method was effective in the analysis of stripline, wire transmission line, microstrip and a strip-fed microstrip patch antenna and, in [3], with equal effectiveness, to lossless and lossy coaxial structures and to wires embedded in a lossy medium.

In this contribution, the approach is extended to allow the treatment of single and multiple 90° and 270° corners in microstrip. These occur frequently in microwave and digital circuits, patch antennas and other microstrip components. A semi-analytical method of calculating the MAMPs for these cases is presented.

The effectiveness of the technique is demonstrated by examining two microstrip patch antennas. One is a "classical" inset patch antenna and the other one contains rectangular holes with dimensions optimized by a genetic algorithm in order to improve the performance [4]. It is shown that the convergence of the calculated results as the mesh size is reduced is greatly improved by using MAMPs for the microstrip corners and that the use of MAMPs allows a much larger cell size to be used while maintaining the same accuracy.

Manuscript received June 27, 2006; revised December 21, 2006.

The authors are with the Centre for Communications Research, University of Bristol, Merchant Venturers Building, Bristol BS8 1UB, U.K. (e-mail: chris.railton@bristol.ac.uk; d.l.paul@bristol.ac.uk, ian.craddock@bristol.ac.uk; geoff.hilton@bristol.ac.uk).

Digital Object Identifier 10.1109/TAP.2007.900270

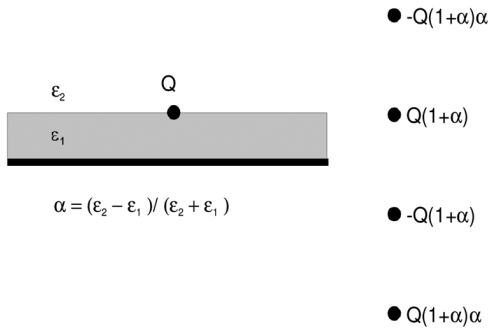

Fig. 1. A planar structure, shown on the left, can be represented by an equivalent structure consisting of an array of images and no dielectric, shown on the right.

II. Calculation of MAMPs for 90° Corner

The general principle behind the use of MAMPs is given in detail in [2] where it was shown that the presence of a metal structure such as a thin wire or microstrip edge within an FDTD cell could be accounted for by modifying the assigned material parameters associated with the cell. The update equations are expressed as in (1), shown at the bottom of the page where the modified material parameter, ε_x, can be expressed in meters as

$$\varepsilon_x = \frac{\langle\langle E_x\rangle\rangle_{yz}}{\langle E_x\rangle_x} \tag{2}$$

For a planar structure where there are one or more dielectric layers above a reflective ground plane, with metallization at a dielectric interface, use can be made of an equivalent structure consisting of an array of images [5]. This is illustrated in Fig. 1 for the case of a single charge element where the first three images are shown on the right. By using this equivalent structure, possible problems arising from field discontinuities at the dielectric boundaries are avoided. In this work only the first image is taken into account as this has been found to give good results and the MAMPs remain independent of the permittivity of the dielectric. If greater accuracy is required then the inclusion of more images would be straight forward.

A. E Field MAMPs

Following (2), the MAMP applicable to the E_y node above a corner in a microstrip can be written as (3) where the quantities, δx, βx, etc. are defined in Fig. 2(a). In this figure, the gray area is metal, the white area is free space and the FDTD nodes in the plane of the metal are shown. For convenience, the origin of coordinates used for the integrals is at the microstrip corner, rather than the FDTD cell corner, so that the nearest E_y node is at coordinates. $(\beta_x\delta_x, \beta_z\delta_z)$ and the nearest H_y node is at coordinates $((\beta_x - 0.5)\delta_x, (\beta_z - 0.5)\delta_z)$

$$\varepsilon_y^+ = \frac{\int_{-\delta x/2+\beta_x\delta x}^{\delta x/2+\beta_x\delta x}\int_{-\delta z/2+\beta_z\delta z}^{\delta z/2+\beta_z\delta z} E_y\left(x, \frac{\delta y}{2}, z\right) dz\, dx}{\int_0^{\delta y} E_y\left(\beta_x\delta x, y, \beta_z\delta z\right) dy} \tag{3}$$

$$\frac{\partial}{\partial t}\langle E_x(i+0.5,j,k)\rangle_x = \frac{1}{\varepsilon\varepsilon_x\delta y\delta z}\begin{pmatrix} \delta y(\langle H_y(i+0.5,j,k-0.5)\rangle_y & -\langle H_y(i+0.5,j,k+0.5)\rangle_y) \\ -\delta z(\langle H_z(i+0.5,j-0.5,k)\rangle_z & -\langle H_z(i+0.5,j+0.5,k)\rangle_z) \end{pmatrix} \tag{1}$$

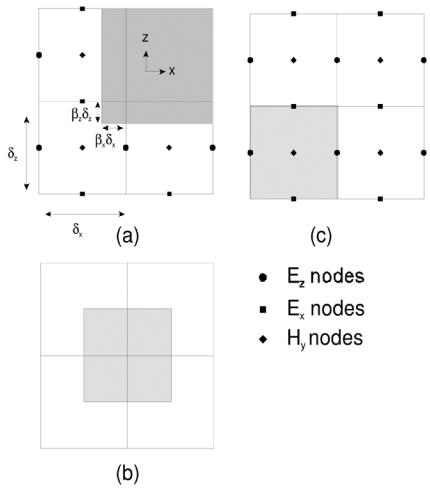

Fig. 2. (a) The position of the 90° corner with respect to the FDTD mesh. (b) The area for the surface integration of E_y, half a cell above or below the patch. (c) The area for the surface integration of H_y.

The area over which the surface integral is required is shown in Fig. 2(b).

In a similar way, the MAMP applicable to the E_y node below the corner is given as follows:

$$\varepsilon_y^- = \frac{\int_{-\delta x/2+\beta_x\delta x}^{\delta x/2+\beta_x\delta x}\int_{-\delta z/2+\beta_z\delta z}^{\delta z/2+\beta_z\delta z} E_y\left(x,-\frac{\delta y}{2},z\right)dzdx}{\int_{-\delta y}^{0} E_y\left(\beta_x\delta x,y,\beta_z\delta z\right)dy}. \quad (4)$$

The MAMP applicable to the H_y node nearest to the corner is given in (5) and the surface of integration is shown in Fig. 2(c)

$$\mu_y = \frac{\int_{-\delta x+\beta_x\delta x}^{\beta_x\delta x}\int_{-\delta z+\beta_z\delta z}^{\beta_z\delta z} H_y\left(x,0,z\right)dzdx}{\int_{-\delta y/2}^{\delta y/2} H_y\left(\frac{\delta x}{2}+\beta_x\delta x,y,\frac{\delta z}{2}+\beta_z\delta z\right)dy}. \quad (5)$$

In order to evaluate these parameters, it is necessary to know the field distribution within a cubical volume surrounding the corner. This can be found either empirically, in a similar manner to that described in [1], or by means of analytic formulae.

It has been shown, e.g., [6], [7], that the surface charge density on an isolated 90° corner in microstrip, as shown in Fig. 2(a), can be approximated as follows:

$$\sigma_{90}\left(r',\theta'\right) \propto \frac{\left(r'\right)^{\nu-1}}{\sqrt{\sin\left(2\theta'\right)}} \quad 0<\theta'<\frac{\pi}{2} \quad (6)$$

where $\nu = 0.297$, the origin of the polar coordinates is at the microstrip corner and the metal exists in the positive quarter-plane.

Thus the electric scalar potential from a corner in free space is given by

$$\phi_{90i}\left(x,y,z\right) \propto \int_0^\infty\int_0^{\pi/2} \sigma_{90}\left(r',\theta'\right) \times \frac{1}{\sqrt{\left(x-r'\cos\left(\theta'\right)\right)^2+\left(z-r'\sin\left(\theta'\right)\right)^2+y^2}} d\theta' dr'. \quad (7)$$

When the corner is on a dielectric substrate of height, h, and dielectric constant, ϵ_r, the total potential is given by the sum over all the partial images

$$\phi_{90}\left(x,y,z\right) = \sum_{n=0}^{N}\left(-\alpha\right)^n \times\left(\phi_{90i}\left(x,y+2nh,z\right)-\phi_{90i}\left(x,y+2\left(n+1\right)h,z\right)\right) \quad (8)$$

where, $2N+1$ images are taken into account and α is defined in Fig. 1.

The value of the field can be calculated by taking the gradient of the potential. For example, the E_y field component for a corner in free space is given in (9), shown at the bottom of the page

To calculate the MAMP, ε_y^+, for the E_y node above the corner, it is necessary to calculate the surface and line integrals given in (3) and (4). By doing the integral with respect to x analytically it can be shown that the required surface integral of E_y is given by (10), shown at the bottom of the page, where

$$k1\left(\delta x,y,z,r',\theta'\right) = \frac{y}{\left(z-r'\sin\left(\theta'\right)\right)^2+y^2} \times\left(\begin{array}{c} \frac{r'\cos\left(\theta'\right)-\frac{\delta x}{2}+\beta_x\delta x}{\sqrt{\left(r'\cos(\theta')-\frac{\delta x}{2}+\beta_x\delta x\right)^2+(r'\sin(\theta')-z)^2+y^2}} \\ -\frac{r'\cos\left(\theta'\right)+\frac{\delta x}{2}+\beta_x\delta x}{\sqrt{\left(r'\cos(\theta')+\frac{\delta x}{2}+\beta_x\delta x\right)^2+(r'\sin(\theta')-z)^2+y^2}} \end{array}\right). \quad (11)$$

$$E_{yi}\left(x,y,z\right) \propto \int_0^\infty\int_0^{\pi/2} \sigma_{90}\left(r',\theta'\right)\frac{y}{\left(\left(x-r'\cos\left(\theta'\right)\right)^2+\left(z-r'\sin\left(\theta'\right)\right)^2+y^2\right)^{1.5}} d\theta' dr'. \quad (9)$$

$$\begin{aligned} &\int_{-\delta z/2+\beta_z\delta z}^{\delta z/2+\beta_z\delta z}\int_{-\delta x/2+\beta_x\delta x}^{\delta x/2+\beta_x\delta x} E_y\left(x,\frac{dy}{2},z\right)dxdz \\ &\propto \int_0^\infty\int_0^{\pi/2}\sigma_{90}\left(r',\theta'\right)\left(\int_{-\delta z/2+\beta_z\delta z}^{\delta z/2+\beta_z\delta z}\sum_{n=0}^{N}\left(-\alpha\right)^n k1\left(\delta x,\frac{dy}{2}+2nh,z,r',\theta'\right)dz\right)d\theta' dr' \\ &\quad -\int_0^\infty\int_0^{\pi/2}\sigma_{90}\left(r',\theta'\right)\left(\int_{-\delta z/2+\beta_z\delta z}^{\delta z/2+\beta_z\delta z}\sum_{n=0}^{N}\left(-\alpha\right)^n k1\left(\delta x,\frac{dy}{2}+2\left(n+1\right)h,z,r',\theta'\right)dz\right)d\theta' dr' \end{aligned} \quad (10)$$

The line integral of E_y for ε_y^+ is given as

$$\int_0^{\delta y} E_y\left(-\beta_x\delta x, \frac{dy}{2}, -\beta_z\delta z\right) dy = \phi_{90}\left(\beta_x\delta x, dy, \beta_z\delta z\right) - \phi_{90}\left(\beta_x\delta x, 0, \beta_z\delta z\right). \quad (12)$$

Substituting the results of (10) and (12) into (3) and (4) and integrating numerically gives the required MAMPs.

B. H Field MAMPs

Analogously with (6), the equivalent magnetic charge in the vicinity of the 90° corner can be written as: [7], [8]

$$\sigma_{90m}\left(r', \theta'\right) \propto H_y\left(r', \theta'\right) \propto \left(r'\right)^{\nu-1} \frac{3\pi}{4} \le \theta' \le \frac{7\pi}{4}$$
$$\sigma_{90m}\left(r', \theta'\right) \propto H_y\left(r', \theta'\right) \propto \frac{\left(r'\right)^{\nu-1}}{\sqrt{\sin\left(2\theta'\right)}} \left(\frac{\pi}{2} \le \theta' \le \frac{7\pi}{4}\right) \vee \left(\frac{3\pi}{4} \le \theta' \le 2\pi\right) \quad (13)$$

where $\nu = 0.815$

Following the same procedure as the previous section, it can be shown that the required surface integral of H_y for μ_y, shown in Fig. 2(b), is given by (14) at the bottom of the page, where $k2$ is given by

$$k2\left(\delta x, y, z, r', \theta'\right) = \frac{y}{\left(z - r'\sin\left(\theta'\right)\right)^2 + y^2} \times \begin{pmatrix} \frac{r'\cos\left(\theta'\right) - \delta x + \beta_x\delta x}{\sqrt{\left(r'\cos\left(\theta'\right) - \delta x + \beta_x\delta x\right)^2 + \left(r'\sin\left(\theta'\right) - z\right)^2 + y^2}} \\ -\frac{r'\sin\left(\theta'\right) + \beta_x\delta x}{\sqrt{\left(r'\cos\left(\theta'\right) + \beta_x\delta x\right)^2 + \left(r'\sin\left(\theta'\right) - z\right)^2 + y^2}} \end{pmatrix}. \quad (15)$$

The line integral of H_y for μ_y is given by

$$\int_{-\delta y/2}^{\delta y/2} H_y\left(-\left(\beta_x + 0.5\right)\delta x, 0, -\left(\beta_z + 0.5\right)\delta z\right) dy = \phi_{90m}\left(\left(\beta_x + 0.5\right)\delta x, \frac{\delta y}{2}, \left(\beta_z + 0.5\right)\delta z\right) - \phi_{90m}\left(\left(\beta_x + 0.5\right)\delta x, -\frac{\delta y}{2}, \left(\beta_z + 0.5\right)\delta z\right) \quad (16)$$

where

$$\phi_{90m}\left(x, y, z\right) = \sum_{n=0}^{N} \left(-\alpha\right)^n \left(\phi_{90mi}\left(x, y + 2nh, z\right) - \phi_{90mi}\left(x, y + 2\left(n+1\right)h, z\right)\right) \quad (17)$$

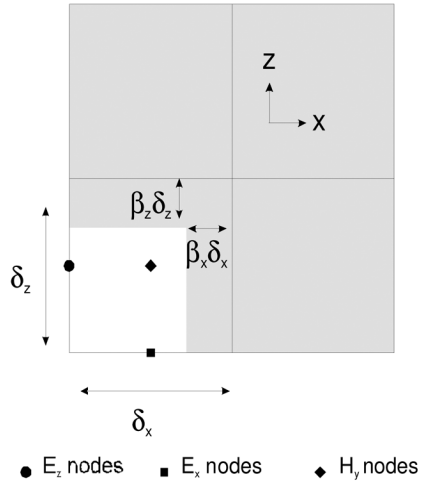

Fig. 3. The position of the 270° corner with respect to the FDTD mesh. The metal area is shown as gray.

and

$$\phi_{90mi}\left(x, y, z\right) \propto \int_0^{\infty} \int_{\pi/2}^{2\pi} \sigma_{90m}\left(r', \theta'\right) \times \frac{1}{\sqrt{\left(x - r'\cos\left(\theta'\right)\right)^2 + \left(z - r'\sin\left(\theta'\right)\right)^2 + y^2}} d\theta' dr'. \quad (18)$$

Substituting (14) and (16) into (5) and integrating numerically gives the required MAMPs for H_y.

III. Calculation of MAMPs for 270° Corner

Calculation of the MAMPs for the 270° corner, shown in Fig. 3, follows the same procedure as for the 90° corner. From [6], [7], the surface charge density on a 270° corner in microstrip can be approximated as

$$\sigma_{270}\left(r', \theta'\right) \propto \left(r'\right)^{\nu-1} - \frac{\pi}{4} \le \theta' \le \frac{3\pi}{4}$$
$$\sigma_{270}\left(r', \theta'\right) \propto \frac{\left(r'\right)^{\nu-1}}{\sqrt{\sin\left(2\theta'\right)}} \left(-\frac{\pi}{2} \le \theta' \le -\frac{\pi}{4}\right) \vee \left(\frac{3\pi}{4} \le \theta' \le \pi\right) \quad (19)$$

where $\nu = 0.815$, the origin of coordinates is at the microstrip corner and the metal exists everywhere except in the negative quarter-plane.

$$\int_{-\delta z + \beta_z\delta z}^{\beta_z\delta z} \int_{-\delta x + \beta_x\delta x}^{\beta_x\delta x} H_y\left(x, 0, z\right) dx dz \propto \int_0^{\infty} \int_{\pi/2}^{2\pi} \sigma_{90m}\left(r', \theta'\right) \left(\int_{-\delta z + \beta_z\delta z}^{\beta_z\delta z} \sum_{n=0}^{N} \left(-\alpha\right)^n k2\left(\delta x, 2nh, z, r', \theta'\right) dz\right) d\theta' dr' - \int_0^{\infty} \int_{\pi/2}^{2\pi} \sigma_{90m}\left(r', \theta'\right) \left(\int_{-\delta z + \beta_z\delta z}^{\beta_z\delta z} \sum_{n=0}^{N} \left(-\alpha\right)^n k2\left(\delta x, 2\left(n+1\right)h, z, r', \theta'\right) dz\right) d\theta' dr' \quad (14)$$

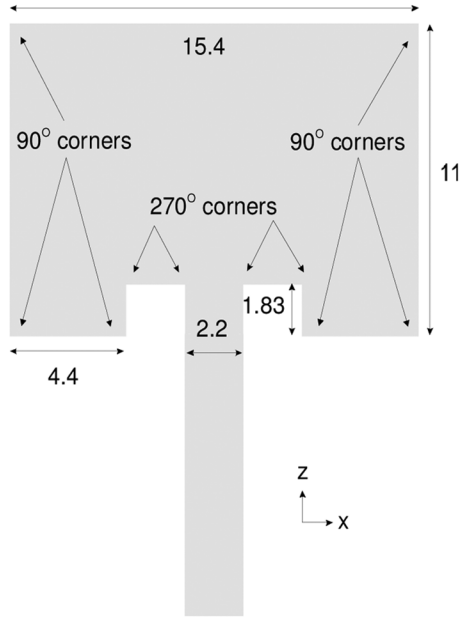

Fig. 4. "Classical" inset patch antenna. Dimensions in millimeters.

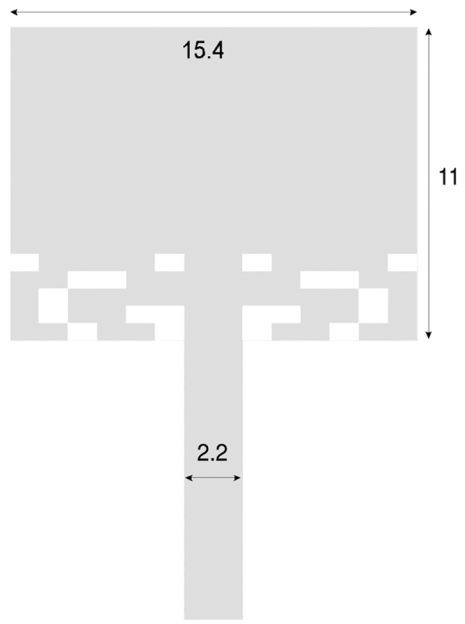

Fig. 5. "GA optimized" patch antenna. Dimensions in millimeters.

Analogously with (7), the electric scalar potential from an isolated corner is written as

$$\phi_{270i}(x,y,z) \propto \int_0^{\infty}\int_{-\pi/2}^{\pi} \sigma_{270}\left(r',\theta'\right) \times \frac{1}{\sqrt{\left(x-r'\cos(\theta')\right)^2+\left(z-r'\sin(\theta')\right)^2+y^2}} d\theta' dr' \quad (20)$$

and the potential from the corner in the presence of the substrate and ground plane is given by

$$\phi_{270}(x,y,z) = \sum_{n=0}^{N}(-\alpha)^n \left(\phi_{270i}(x,y+2nh,z) - \phi_{270i}(x,y+2(n+1)h,z)\right). \quad (21)$$

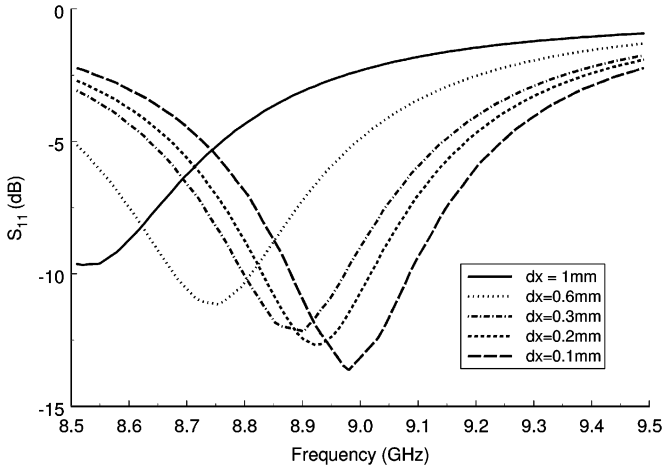

Fig. 6. Inset guide using basic FDTD.

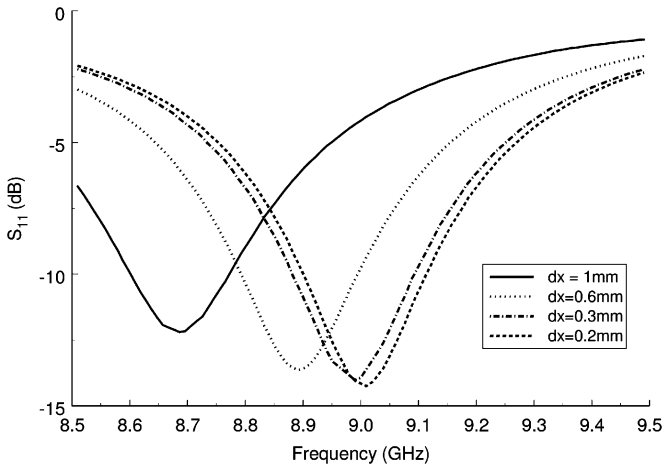

Fig. 7. Inset guide using MAMPs for edges only.

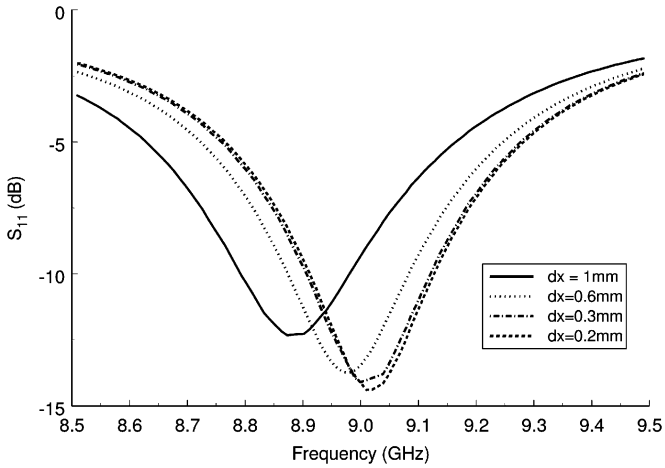

Fig. 8. Inset guide using MAMPs including corners.

The E_y field integrals are given by (22) and (23) shown at the bottom of the following page.

Substituting the results into (3) and integrating numerically gives the required MAMP for ϵ_y^+.

TABLE I
VALUES OF THE MAMPS FOR DIFFERENT CELL ASPECT RATIOS AND $\beta = 0$

Cell aspect ratio	90^0			270^O		
	ε_y^+	ε_y^-	μ_y	ε_y^+	ε_y^-	μ_y
1:1	0.43	0.51	1.24	0.89	0.93	1.8
2:1	0.33	0.44	1.16	0.81	0.92	1.7
3:1	0.26	0.40	1.17	0.73	0.90	1.7
4:1	0.19	0.35	1.21	0.62	0.85	1.7
6:1	0.16	0.28	1.16	0.48	0.87	1.6

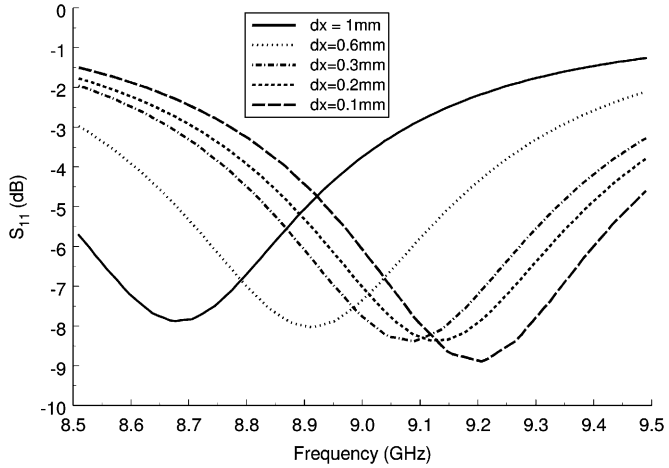

Fig. 9. GA patch using basic FDTD.

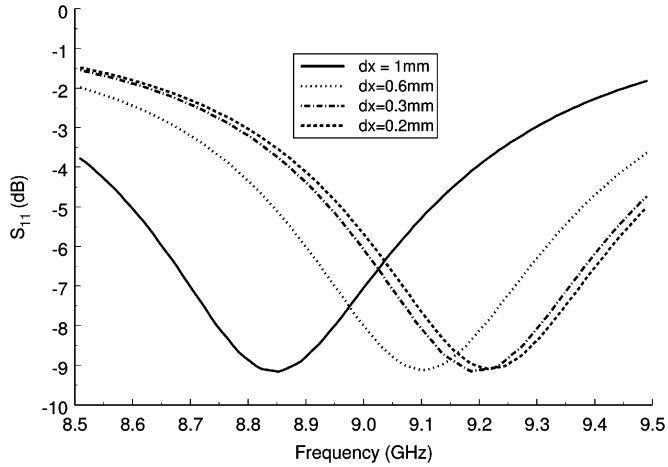

Fig. 10. GA patch using MAMPs for edges only.

IV. RESULTS OBTAINED USING MAMPS

In order to assess the effectiveness of the proposed treatment of corners on a realistic problem, the two patch antennas, designed to operate at around 9.2 GHz and described in [4] were used as test cases. The plan view of these antennas are shown in Figs. 4 and 5. In each case the substrate height is 0.762 mm and its relative permittivity is 2.2. A more detailed description, including all dimensions, can be found in [4]. The "classical" inset patch antenna includes six 90° corners and four 270° corners. The "GA optimized" patch contains many holes in the metallization leading to numerous corners, all of which can be treated with the MAMPs described in this paper. The values for the MAMPs used for these examples are given in Table I for the different cell aspect ratios. In addition, the smallest holes in the metallization have dimensions of 0.61 mm × 1.1 mm so that, for very coarse meshes, individual holes may only be the size of a single cell.

The results for the "classical" inset patch are shown in Figs. 6–8. Fig. 6 shows the results using basic FDTD where it can be seen that there is considerable variation with cell size. In Fig. 7 results are shown for the case where MAMPs are used for the edges but not for the corners. It can be seen that the variation with cell size has been reduced but is still substantial. Finally, in Fig. 8, results are shown for the case where MAMPs are used for edges and corners and it can be seen that the variation with cell size is much reduced. In each case the smallest cell size in the plane of the patch corresponds to $\lambda_g/100$ and the largest cell size corresponds to $\lambda_g/20$ and is the size of the smallest hole in the "GA optimized" patch. In all cases δy was 0.1905 mm.

Results for the "GA optimized" patch are shown in Figs. 9–11. Again it can be seen that the convergence is vastly superior when MAMPs are used compared to when they are not and that, while correcting just for edges improves the convergence, the additional corrections for the corners gives a further substantial increase in accuracy when using coarser

$$\int_{-\delta z/2+\beta_z\delta z}^{\delta z/2+\beta_z\delta z}\int_{-\delta x/2+\beta_x\delta x}^{\delta x/2+\beta_x\delta x} E_y\left(x,\frac{dy}{2},z\right)dxdz$$
$$\propto \int_0^{\infty}\int_{\pi/2}^{2\pi}\sigma_{270}\left(r',\theta'\right)\left(\int_{-\delta z/2+\beta_z\delta z}^{\delta z/2+\beta_z\delta z}\sum_{n=0}^{N}(-\alpha)^n\, k1\left(\delta x,\frac{dy}{2}+2nh,z,r',\theta'\right)dz\right)d\theta' dr'$$
$$-\int_0^{\infty}\int_{\pi/2}^{2\pi}\sigma_{270}\left(r',\theta'\right)\left(\int_{-\delta z/2+\beta_z\delta z}^{\delta z/2+\beta_z\delta z}\sum_{n=0}^{N}(-\alpha)^n\, k1\left(\delta x,\frac{dy}{2}+2\left(n+1\right)h,z,r',\theta'\right)dz\right)d\theta' dr' \tag{22}$$

$$\int_0^{\delta y} E_y\left(-\beta_x\delta x,\frac{dy}{2},-\beta_z\delta z\right)dy = \phi_{270}\left(\beta_x\delta x,dy,\beta_z\delta z\right)-\phi_{270}\left(\beta_x\delta x,0,\beta_z\delta z\right). \tag{23}$$

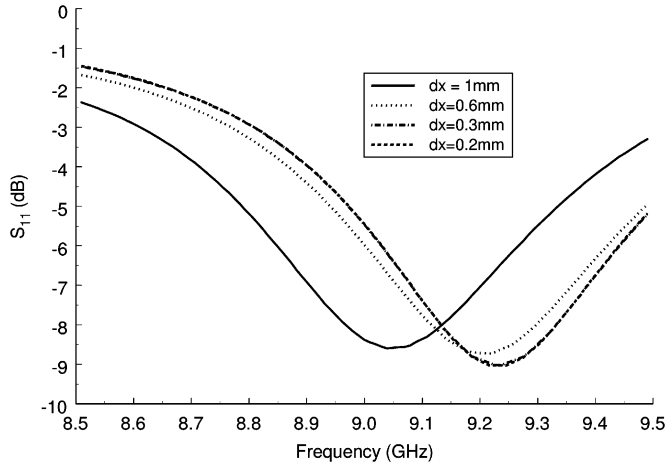

Fig. 11. GA patch with MAMPs including corners.

meshes. The coarsest mesh predicts a lower frequency than the rest but, even so, the result is as good as that obtained using basic FDTD with cells of one third the size.

V. Conclusions

In this contribution it has been shown that 90° and 270° corners in microstrip may be accurately treated in the FDTD method by means of semi-analytically calculated Modified Assigned Material Parameters. It has been shown that a complex patch antenna can be modelled with MAMPs using a much larger cell size than would be needed using standard FDTD in order to achieve the same accuracy.

References

[1] C. J. Railton, "The inclusion of fringing capacitance and inductance in FDTD for the robust accurate treatment of material discontinuities," *IEEE Trans. Microw. Theory Tech.*, vol. 48, pp. 2283–2288, Jan. 2000.

[2] C. J. Railton, D. L. Paul, I. J. Craddock, and G. S. Hilton, "The treatment of geometrically small structures in FDTD by the modification of assigned material parameters," *IEEE Trans. Antennas Propag.*, vol. 53, no. 12, pp. 4129–4136, Dec. 2005.

[3] C. J. Railton, D. L. Paul, and S. Dumanli, "The treatment of thin wire and coaxial structures in lossless and lossy media in FDTD by the modification of assigned material parameters," *IEEE Trans Electromagn. Compat.*, pp. 654–660, Nov. 2006.

[4] [Online]. Available: http://www.antennasvce.org/Community/Dissemination?action=element_view&id_element=67&id_area=19

[5] K. Scott, *The Practical Modelling of Printed Circuit Boards*. New York: Wiley, 1994.

[6] S. Marchetti and T. Rozzi, "Electric field singularities at sharp edges of planar conductors," *IEEE Trans. Antennas Propag.*, vol. AP-39, no. 9, pp. 1312–1320, Sep. 1991.

[7] S. Marchetti, "Wedge diffraction in planar microwave circuits," Ph.D. dissertation, Univ. of Bath, Bath, U.K., 1992.

[8] S. Marchetti and T. Rozzi, "H-field and J-current singularities at sharp edges of printed circuits," *IEEE Trans. Antennas Propag.*, vol. AP-39, no. 9, pp. 1321–1331, Sep. 1991.

Characterization of the 60 GHz Wireless Desktop Channel

C. Liu, E. Skafidas, and R. J. Evans

***Abstract*—We measure and characterize the 55–65 GHz wireless channel for a typical desktop environment. The Saleh–Valenzuela (S-V) model is used to describe the desktop environment. Key S-V model parameters such as cluster decay factor, ray decay factor, cluster arrival rate, and ray arrival rate are extracted from measured data.**

***Index Terms*—Millimeter wave propagation, multiple-path channel, radio propagation.**

I. Introduction

The unlicensed spectrum around 60 GHz became available in recent years in the United States, Europe, Japan, and Australia. This availability has unlocked significant opportunities for developing ubiquitous gigabit wireless connectivity. Significant research activity is now being undertaken to design next-generation high-speed wireless communication systems in this millimeter-wave band. A critical component in the design of these systems is understanding the propagation environment to assist in choosing appropriate modulation and space–time coding schemes.

An important application of millimeter wavelength wireless communication systems capable of multigigabit per second data rates is to connect computer components and peripherals that reside on a desktop. Hence an accurate channel model for a desktop is required. The aim of the measurement campaign described here is to determine the appropriate Saleh–Valenzuela (S-V) model [1], [2] parameters that accurately describe a 60 GHz desktop channel.

In this paper, experiments are developed and executed to measure the 55–65 GHz band wireless channel on typical desktop environments. A single model to represent the typical desktop is determined. This is important for the standardization and research communities where a model is required in order to evaluate performance of different wireless modulation schemes. Here we used a modified S-V model. Key S-V model parameters such as cluster decay factor, ray decay factor, cluster arrival rate, and ray arrival rate are extracted from measured data. It is shown that for the desktop environment, data support the hypothesis that the multiple-path gains are log-normally distributed.

This paper is organized as follows. In Section II, we review the modified S-V model for the desktop propagation environment. In Section III, we introduce our experimental setup. In Section IV, we describe our measurements and present the extracted S-V parameters. Section V concludes this paper.

II. The Modified S-V Model

As stated above, we use a modified S-V model. Following previous work [1], we use a log-normal distribution rather than a Rayleigh distribution for the multipath gain magnitude. Our measurements are shown to support this assumption.

Manuscript received December 22, 2005; revised January 3, 2007.

The authors are with the Department of Electrical and Electronic Engineering, National ICT Australia, University of Melbourne, Victoria 3010, Australia (e-mail: c.liu@ee.unimelb.edu.au; stan.skafidas@nicta.com.au; rob.evans@nicta.com.au).

Color versions of one or more of the figures in this paper are available online at http://ieeexplore.ieee.org.

Digital Object Identifier 10.1109/TAP.2007.900267